

# The Optical Properties of Tropical Cirrus Clouds in the Maritime Continent Thunderstorm Experiment from Lidar and Infrared Radiometer Retrievals

*C.M.R. Platt, S. A. Young, R. T. Austin, G. R. Patterson and S. C. Marsden  
CSIRO, Division of Atmospheric Research  
Aspendale, Victoria, Australia*

## Introduction

Observations of the optical and structural properties of equatorial cirrus clouds were made previously in the Atmospheric Radiation Measurement (ARM) Program's Pilot Radiation Observation Experiment (PROBE) in 1993 and were reported in Platt et al. (1996). The results are presented in final form in Platt et al. (1997).

The Maritime Continent Thunderstorm Experiment (MCTEX) provided another opportunity to study tropical cirrus and anvil clouds. The component of the experiment that included the lidar and radars was supported by the ARM Program. The experiment has provided a further set of data to categorize tropical cirrus in terms of their cloud-radiation interactions, a central theme of the ARM Program. The data also provide additional support to the new ARM Cloud and Radiation Testbed (CART) site on Manus Island by indicating the types of atmospheric conditions likely to be found, together with associated cloud optical properties.

Observation of tropical storm anvils was a priority during MCTEX. It was basically an experiment to follow the life cycles of local island thunderstorms that build up daily over the Tiwi Islands at the start of the monsoon season. This paper presents an analysis of a number of case studies taken at MCTEX.

## Experiment

MCTEX was coordinated by the Australian Bureau of Meteorology, Melbourne, in association with a number of institutes overseas and several universities and government departments within Australia. The participation of the CSIRO Division of Atmospheric Research, the University of Massachusetts, and Pennsylvania State University was supported by the ARM Program.

The ARM component of MCTEX was operated at Pirlangimpi, Melville Island, some 100 km north of Darwin, Northern Territory, at 130.4138°E, 11.3990°S. The CSIRO, Division of Atmospheric Research operated its new three-wavelength lidar at 532 nm and Mark I three-filter CSIRO/ARM narrow-beam radiometer at  $10.86 \pm 0.5 \mu\text{m}$ . The lidar characteristics are given in Austin et al. (1997) in this volume. The radiometer had a time constant of 1 second and an aperture of 8 milliradians, compatible with the lidar. The instruments were situated within 2 meters of each other in the lidar caravan and aligned carefully in the vertical to observe simultaneously the same volume of cloud. The lidar caravan was situated close to the University of Massachusetts' two-frequency millimeter radar and the National Oceanic and Atmospheric Administration's S-band radar (see Austin et al. [1997]). A two-frequency microwave radiometer was also situated within about 10 meters of both instruments.

Observations were made of both isolated cirrus and thunderstorm anvils. Cirrus was present for most of the experiment. Observations were restricted at times by the presence of attenuating cumulus and mid-level altocumulus clouds. The former tended to build up during the morning and early afternoon. Observations were made mostly during daytime, but some late night and early morning observations were also made.

In total, some 132 hours of lidar and radiometer data were obtained. This paper presents some case studies, together with some preliminary results from a subset of the data.

## Analysis

As in previous studies (i.e., Platt et al. 1987, 1997), the analysis consisted of obtaining lidar cloud integrated attenuated backscatter  $\gamma'(\pi)$  and relating this to the cloud infrared (IR) absorption emittance  $\epsilon_a$ .

$$\gamma'(\pi) = \frac{\kappa}{2\eta} \left[ 1 - \exp\left(-2\eta\alpha \log \frac{1}{1-\epsilon_a}\right) \right] \quad (1)$$

where  $\kappa$  is the cloud isotropic backscatter to extinction ratio,  $\eta$  is a multiple scattering factor, and  $\alpha$  is the ratio between the lidar visible extinction coefficient and the infrared absorption coefficient.

The cloud boundaries for each lidar backscatter profile are retrieved with a threshold method described by Young (1995). The boundaries are determined by using two “windows” above and below the cloud, respectively, where the lidar profile is fitted to a reference molecular backscatter profile. A threshold technique is then applied to detect the actual cloud boundaries. An example of the retrieved cloud boundaries of a cirrus cloud in MCTEX is shown in Figure 1. It is intended to automate this method for near-real-time retrieval of cirrus cloud parameters.

The cloud infrared radiance as measured at the surface is modified by water vapour radiance and absorption. The cloud radiance  $L_c$  is retrieved using

$$L_c = \frac{L_s - I_{sky}}{\tau} \quad (2)$$

where  $L_s$  is measured radiance,  $I_{sky}$  is water vapour radiance from the cloudless sky, and  $\tau$  is the transmittance of water vapour between the cloud and ground. It is assumed that, for cirrus clouds, all water vapour resides below the clouds. The water vapour radiance and transmittance can be calculated with a radiative transfer equation together with radiosonde data. The radiance can also be measured during cloudless periods and compared with the calculated radiance. The relationship of the transmittance to the radiance is shown in Figure 2 for the range of conditions pertaining to MCTEX. The points were generated from calculations using the radiosonde data obtained during the entire experiment. A number of absorption models were used for each radiosonde ascent. It can be seen that, for the moist tropical atmospheres encountered, the radiance was quite high and the transmittance, at certain times, was quite low. This was a similar result as obtained during PROBE by Platt et al. (1996, 1997). The close correlation indicates that the temperature of the atmosphere where the water vapour emission peaked did not change significantly during the experiment

During both PROBE and MCTEX, the integrated water vapour path observed by the microwave radiometer fluctuated considerably during observations. This implied that the water vapour radiance also varied; and during observations with a

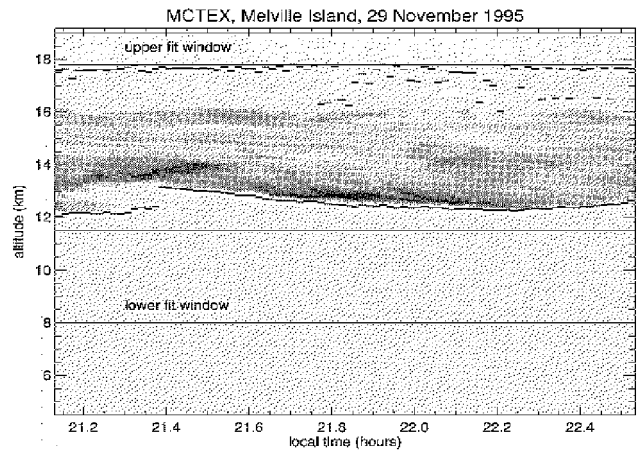


**Figure 1.** Time-height diagram of lidar backscatter for a cirrus cloud at MCTEX, showing retrieved cloud boundaries, indicated by ‘-’ bars.

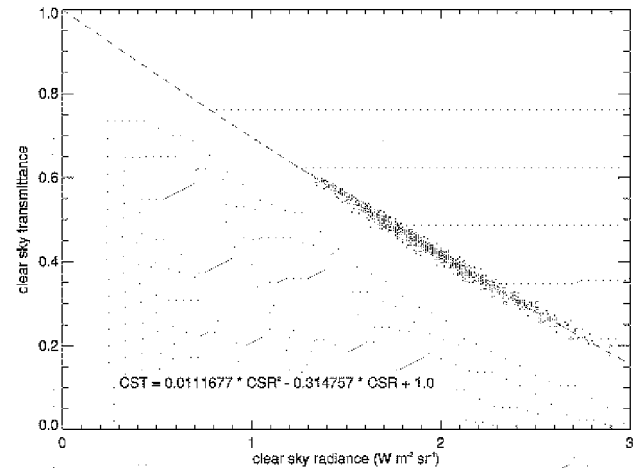


**Figure 2.** Plot of water vapour transmittance versus radiance at 10.86  $\mu\text{m}$  wavelength calculated from MCTEX radiosonde data.

clear sky or with very thin cirrus, this variability was apparent. Such observations are shown clearly in Figures 3a and 3b, which illustrate a lidar time-height plot and a plot of infrared radiance and integrated water vapour path, against time. When the cloud is very thin and high (cold), the cloud radiance reaching the ground will be small and the radiance variations follow those of the water path quite closely. When thicker cloud intervenes, then the radiance increases faster than the water path. These diagrams indicate that subtraction of the water vapour effects is essential in order to retrieve accurate cloud data.

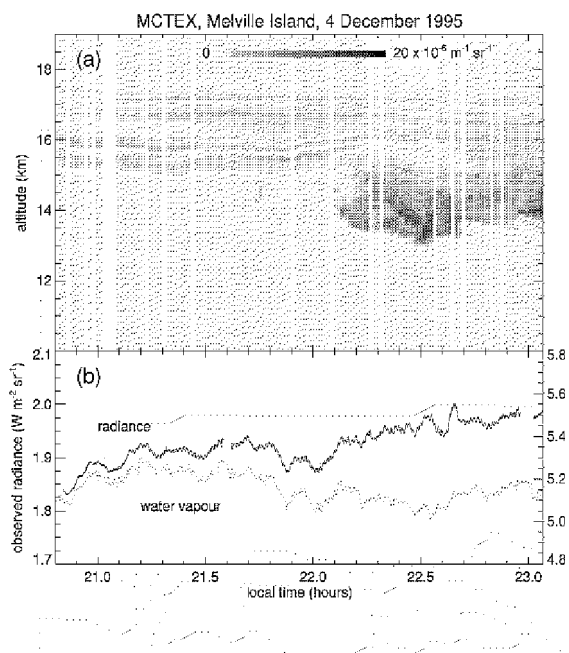


**Figure 3.** (a) Time-height diagram of lidar attenuated backscatter for one cirrus case. (b) Corresponding infrared radiance and integrated water vapour path.

The cloud emittance  $\epsilon_a$  is calculated as described in Platt et al. (1987, 1997). First, the lidar backscatter coefficients are corrected for attenuation at every level in the cloud profile at which they were recorded. An infrared absorption coefficient is then assigned to each lidar backscatter coefficient through a ratio  $\xi$ . The cloud radiance at the surface is then computed, employing effective filter blackbody radiances calculated from a radiosonde temperature profile.  $\xi$  is then adjusted until the calculated and observed radiances are equal. The absorption coefficients are then integrated through the cloud to give an absorption optical depth  $\delta_a$ . Then  $\epsilon_a$  is calculated as

$$\epsilon_a = 1 - \exp(-\delta_a) \quad (3)$$

## Results

Figures 4a, 4b, and 4c illustrate a case study on December 5, 1995. In this case, the cloud is moderately dense and the IR emittance reaches maximum values of 0.6. There is a relatively tight relationship between  $\gamma'(\pi)$  and  $\epsilon_a$ , which is what is predicted by (1) and by previous results (e.g., Platt et al. 1987). Figure 4c indicates that variations in radiance due to variations in water path once again need to be subtracted.

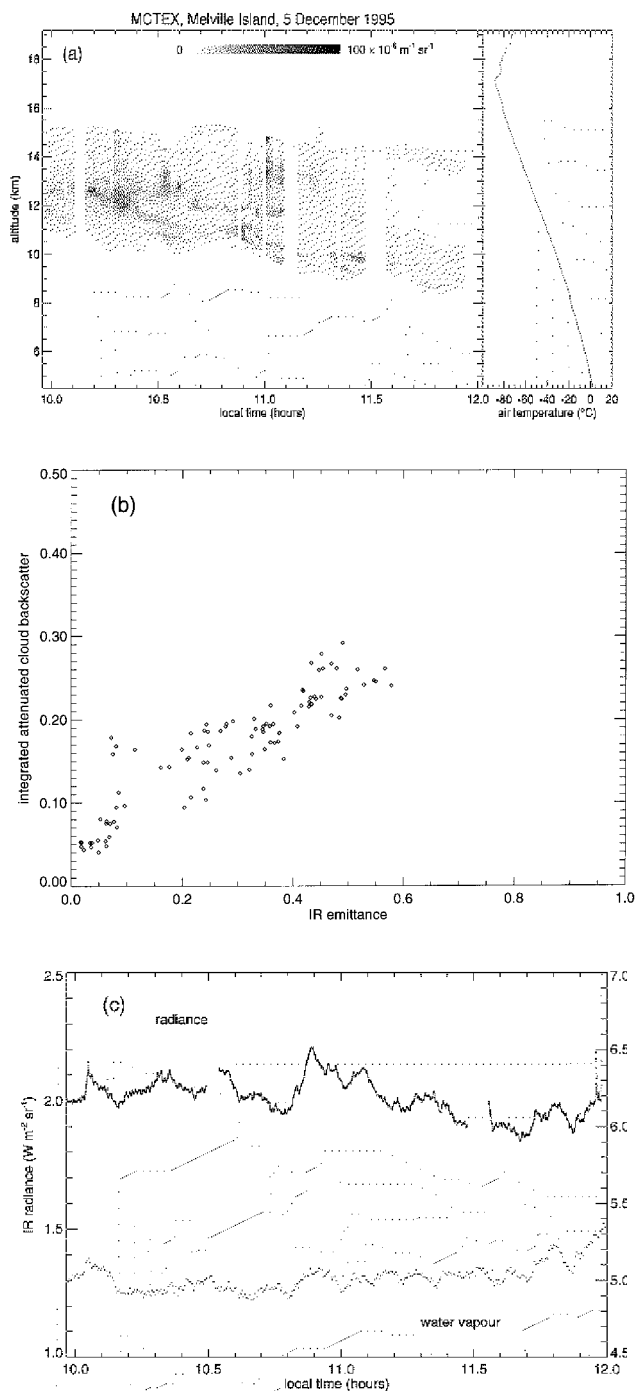


**Figure 4.** (a) Time-height diagram of lidar backscatter for medium density cirrus. (b) Plot of integrated attenuated lidar backscatter versus emittance. (c) Corresponding infrared radiance and water vapour path.

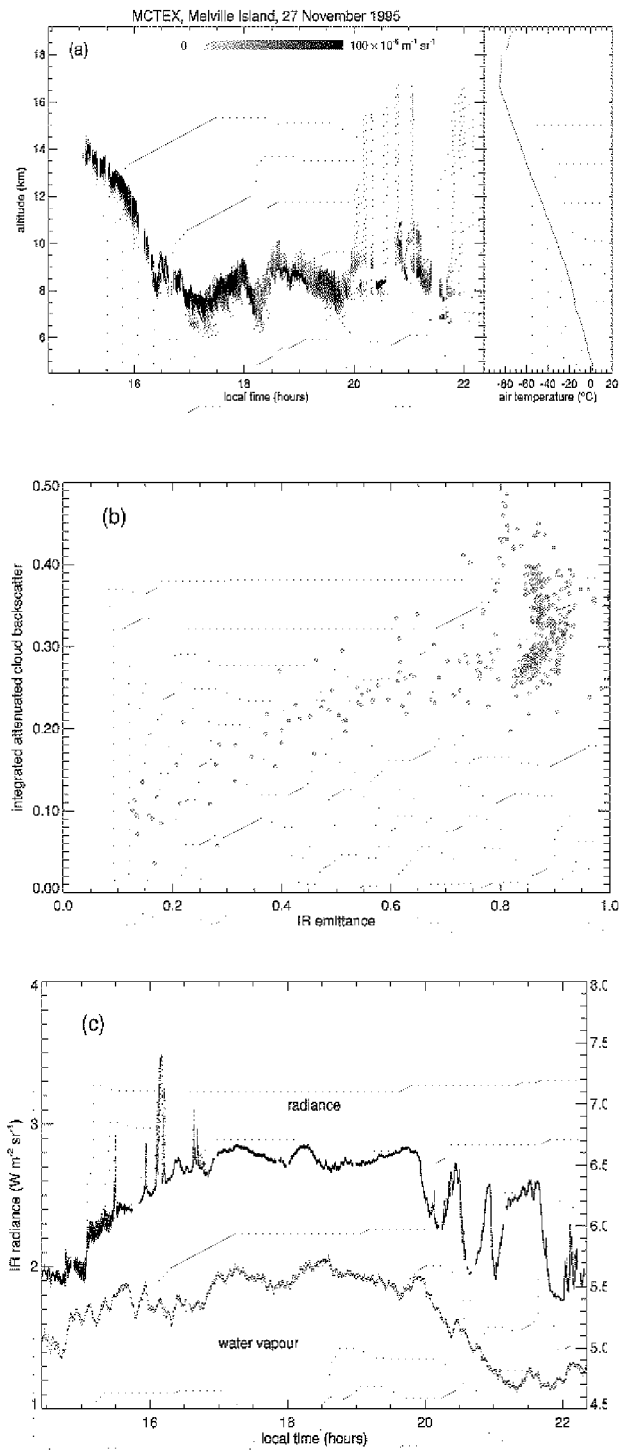


**Figure 5.** (a) Time-height diagram of corrected lidar backscatter coefficient for a storm anvil. (b) Plot of integrated attenuated lidar backscatter versus emittance. (c) Infrared radiance and water vapour path.

In Figure 4b, when the emittance is just less than 0.1, there are four lidar shots with anomalously high values of integrated attenuated backscatter. These shots were sequential, occurring just before 1130 local time (see Figure 4a). The high values are due probably to reflection from horizontally oriented crystals (e.g., see Platt et al. 1987).

A rather different case of a thunderstorm anvil is shown in Figures 5a, 5b, and 5c. The time-height backscatter intensity image shown in Figure 5a indicates the strong attenuation experienced by the lidar pulse in the dense anvil cloud. Millimeter radar data (see Austin et al. 1997) indicated that the cloud top remains at about 14 km throughout the observation time. After 2000 hrs, the cloud starts to break up and become semitransparent to the infrared radiation. This is reflected by the spread in the values of emittance in the plot of  $\gamma'(\pi)$  versus  $\epsilon_a$  illustrated in Figure 5b. The spikes on the radiance curve in Figure 5c are due to small cumulus clouds crossing the field of view of the radiometer. It is interesting that the water vapour path increases at the time that the anvil is passing over and then decreases sharply when the anvil is dissipating. This may be due partly to the presence of a deep moist layer in the anvil itself. However, the presence of liquid water in the cloud could also cause erroneously high values of water vapor. This possibility is under investigation at present.

Finally, Figure 6 shows some values of  $\epsilon_a$  plotted against mid-cloud temperature from an analyzed subset of the

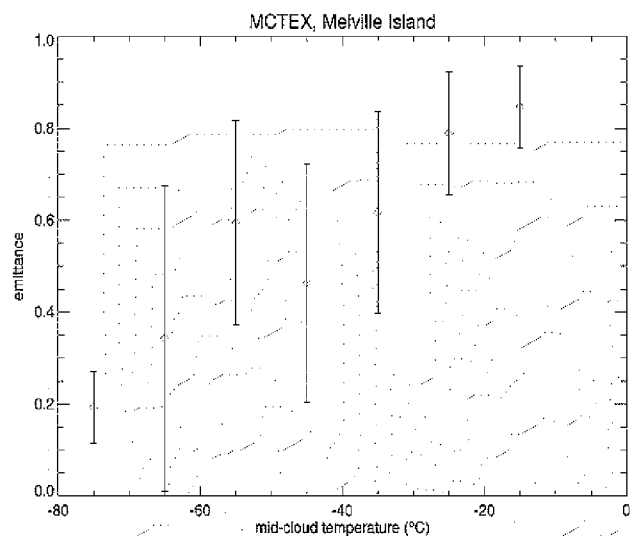


**Figure 6.** Infrared emittance for all cloud cases within specified temperature bins for a subset of the MCTEX data. Bars represent variations in the data ( $\pm 1$  s.d.) rather than errors in the retrievals.

MCTEX data. The values and temperature dependence of  $\epsilon_a$  are very similar to those obtained at other locations (e.g., Platt et al. 1987, 1997).

## Summary

The case studies shown here indicate the range of ice clouds and storm anvils that were observed at the MCTEX site. This is a different site to that at Kavieng, which was only 2°S of the Equator. The MCTEX site was slightly drier than Kavieng, but still very moist.

The data should be valuable for modeling the cirrus cloud and storm processes that were observed. One significant observation was the frequent occurrence of thin cirrus layers just below the tropopause. These layers have been suspected to exist both from satellite and other data. They were also present during PROBE (Platt et al. 1997). They are very important to the radiation budget at the top of the atmosphere. Lidar observations at the new ARM site on Manus Island, Papua New Guinea (PNG), should help to further elucidate their properties.

## Acknowledgments

The authors thank the Bureau of Meteorology MCTEX Science Team for their logistical support of the ARM component of the experiment. The research was supported under the U.S. Department of Energy, Office of Health and Environmental Research, Grant No DE-FG02-92ER61373.

## References

- Austin, R. T., S. A. Young, C.M.R. Platt, G. R. Patterson, S. M. Sekelsly, and R. E. McIntosh, 1997: Retrieval of tropical cirrus cloud properties from ground-based lidar and millimeter-wave radar sensing at MCTEX. *Proceedings of the Seventh Atmospheric Radiation Measurement (ARM) Science Team Meeting, March 3-7, 1997, San Antonio, Texas.* CONF-970365, U.S. Department of Energy, Washington, D.C.
- Platt, C.M.R., J. C. Scott, and A. C. Dilley, 1987: Remote sounding of high clouds, Part VI: Optical properties of mid-latitude and tropical cirrus. *J. Atmos. Sci.*, **44**, 729-747.
- Platt, C.M.R., S. A. Young, R. T. Austin, S. C. Marsden, G. R. Patterson, J. A. Bennett, B. Petraitis and B. Turner, 1996: Retrieval of cloud properties from ground-based lidar/radiometer data. *Proceedings of the Sixth Atmospheric Radiation Measurement (ARM) Science Team Meeting, March 4-7, 1996, San Antonio, Texas*, pp. 265-269. CONF-9603149, U.S. Department of Energy, Washington, D.C.
- Platt, C.M.R., S. A. Young, P. J. Manson, G. R. Patterson, S. C. Marsden, R. T. Austin, and J. Churnside, 1997: The optical properties of equatorial cirrus from observations in the ARM Pilot Radiation Observation Experiment. *J. Atmos. Sci.* (submitted).
- Young, S. A., 1995: Analysis of lidar backscatter profiles in optically thin clouds. *Appl. Opt.*, **34**, 7019-7031.